Journal of Building Engineering 89 (2024) 109401

Contents lists available at ScienceDirect

Journal of Building Engineering

journal homepage: www.elsevier.com/locate/jobe

Full length article

Hierarchical-stochastic model predictive control for a grid-interactive multi-zone residential building with distributed energy resources

Felix Langner [a,*], Moritz Frahm [a], Weimin Wang [b], Jörg Matthes [a], Veit Hagenmeyer [a]

[a] Institute for Automation and Applied Informatics, Karlsruhe Institute of Technology, Eggenstein-Leopoldshafen, 76344, Germany
[b] Department of Engineering Technology, University of North Carolina at Charlotte, Charlotte, 28223, NC, United States

ARTICLE INFO

Keywords:
Hierarchical model predictive control
Building energy management
Uncertainty analysis
Model predictive control
Energy efficiency

ABSTRACT

Using Model Predictive Control (MPC) is a promising method for enabling grid-interactive efficient buildings. Since MPC relies on a building model and the forecasts of external disturbances to derive optimal inputs, the uncertainties due to forecast errors and model inaccuracies can deteriorate the control performance. Most existing MPC studies for the built environment are deterministic MPC without consideration of uncertainties even though several different methods (e.g., stochastic MPC) are available in the literature to deal with them. Even studies that consider forecast uncertainties often neglect model inaccuracies. Hence, in the present paper, a novel hierarchical-stochastic MPC is proposed considering forecast uncertainties and model inaccuracies, and its performance is compared with deterministic, stochastic, and hierarchical MPC for power management in a residential building with distributed energy resources. The control objective is the cost-optimal scheduling of a heat pump, a battery for energy storage, and a rooftop photovoltaic system. Measurement data is used to identify the building model. The results for one-week simulation in winter show that (1) the deterministic MPC results in an unacceptable level of temperature constraint violations in two out of five rooms; (2) the hierarchical MPC can reduce the temperature constraint violations to an acceptable level at the expense of increased cost; (3) the stochastic MPC achieves the same reduction in temperature constraint violations as the hierarchical MPC but at slightly lower costs; and (4) the new proposed hierarchical-stochastic MPC results in both lower temperature constraint violations and lower financial expenses than the use of stochastic or hierarchical MPC individually.

1. Introduction

Buildings consume approximately 40% of the final energy in the EU, two-thirds of which is used for Heating, Ventilation, and Air Conditioning (HVAC) [1]. At the same time, the increasing penetration of intermittent power generation from renewable sources challenges the reliable grid operation that must balance power supply and demand continuously [2]. Flexible operation of HVAC systems can contribute to balancing power supply and demand [2]. As a promising approach to shifting the power consumption in buildings to grid-supportive times, MPC has attracted considerable attention in research (e.g., [3–8]). MPC solves a constrained optimization problem over a prediction horizon based on a building model and the forecasts of external disturbances (e.g., weather forecasts or occupant behavior). Compared to conventional control, MPC can provide flexibility services while simultaneously

* Corresponding author.
E-mail address: felix.langner@kit.edu (F. Langner).

https://doi.org/10.1016/j.jobe.2024.109401
Received 29 November 2023; Received in revised form 8 April 2024; Accepted 17 April 2024
Available online 20 April 2024

Nomenclature

Acronyms

DMPC	Deterministic Model Predictive Control
HMPC	Hierarchical Model Predictive Control
HSMPC	Hierarchical-Stochastic Model Predictive Control
HVAC	Heating, Ventilation, and Air Conditioning
KPI	Key Performance Indicator
MPC	Model Predictive Control
PMPC	Piloting Model Predictive Control
PV	Photovoltaic
SMPC	Stochastic Model Predictive Control

Binary variables

$s_{\text{buy}}, s_{\text{sell}}$	Describe if power is purchased or sold
$s_{\text{d}}, s_{\text{ch}}$	Describe if battery is (dis-)charged

Continuous variables

Δ_{comfort}	Metric to assess the temperature constraint violations
$\dot{q}_{\text{s}}$	Solar radiation
$\dot{Q}_{\text{h}}$	Emitted heat flow by the heat pump
$\hat{P}_{\text{buy}}$	Power to be purchased as scheduled by the scheduling MPC
$\hat{x}$	States estimated by the Kalman filter
$\mathbf{W}$	Covariance matrix of SMPC
ε	Coefficient of performance of the heat pump
ξ	Slack variable for the temperature constraints
$cost$	Metric to assess the financial expenses
E	Stored energy in the battery
P_{buy}	Purchased power from the grid
$P_{\text{d}}, P_{\text{ch}}$	(Dis-)charging power of the battery
P_{HP}	Power consumption of the heat pump
P_{PV}	Power generated by the photovoltaic system
P_{sell}	Sold power to the grid
$RMSE$	Root mean square error
SOC	State of charge of the battery
T_{a}	Ambient air temperature
T_{i}	Indoor air temperature
T_{m}	Temperature of the thermal mass
u	Inputs
w	Process noise
x	States
z	Disturbances

Parameters

α	Probability of temperature constraint violations in SMPC
$\eta_{\text{d}}, \eta_{\text{ch}}$	(Dis-)charging efficiency of the battery
γ	Factor to penalize the temperature constraint violations
Ω_{buy}	Dynamic electricity price signal
Ω_{sell}	Financial compensation for selling power to the grid
C_{i}	Heat capacity of the indoor air
C_{m}	Heat capacity of the thermal mass

improving thermal comfort [3]. However, uncertainties due to inaccurate building models and erroneous forecasts can deteriorate the control performance and jeopardize constraint satisfaction. In the context of built environment control, uncertainties in MPC, if not addressed properly, can result in compromised thermal comfort for occupants.

g_s	Solar heat gains factor
H_f	Prediction horizon of the PMPC
H_s	Prediction horizon of the MPCs
N	Number of time steps over the prediction horizon
R_a	Thermal resistance between the ambient and indoor air
R_i	Thermal resistance between the indoor air and thermal mass
t_f	Sample time of the PMPC
t_s	Sample time of the MPCs

Various methods have been proposed to address uncertainties in MPC formulations explicitly [3]. For example, stochastic MPC (SMPC) leverages the knowledge of statistical distributions of the uncertain forecast errors to satisfy constraints with a user-defined probability [4]. For this purpose, the constraints are formulated as chance constraints and increasingly tightened over the prediction horizon. In the context of building energy systems, SMPC has been successfully applied to minimize the energy consumption of HVAC systems [4,5], to cost-optimally operate home energy management systems [6,7,9], and to improve the demand flexibility estimate in buildings [8]. The performance of SMPC is frequently benchmarked against a rule-based control [4,7] and deterministic MPC (DMPC) [4–7,9], that treats the optimization problem deterministically by considering the erroneous forecasts as perfect.

In the reviewed studies, the application of SMPC has resulted in reduced temperature constraint violations compared to the benchmark controllers, indicating improved thermal comfort [4–9]. The improved thermal comfort is often achieved at the expense of increased energy use [5,7] or cost [6,7,9]. However, SMPC has also been reported to simultaneously improve the thermal comfort and the control objective (e.g. the energy use) [4,7]. Given the excellent performance of SMPC, Yao et al. [10] stated that SMPC was the most suitable control algorithm for HVAC systems.

Forecast errors and model inaccuracies can also be handled implicitly by selecting a short sample time of the MPC, which results in frequent rescheduling of the optimization problem. However, short sample times combined with large prediction horizons lead to high computational complexity. This can be overcome by establishing a hierarchical control problem, where the upper layer computes the optimal schedule with a large prediction horizon and a large time step while the lower layer tracks the derived schedule and handles deviations with a short time step and a short prediction horizon [3]. The hierarchical MPC (HMPC) has been applied for the control of HVAC systems and thermal energy storage [11], the energy management in residential buildings [12,13], and the temperature control in buildings with thermally activated building systems [14]. Using HMPC has simultaneously improved thermal comfort and reduced electricity costs [12] as well as reduced energy consumption [14] when compared to conventional controls such as rule-based control and proportional–integral control. The merits of HMPC are also compared with centralized (i.e. non-hierarchical) MPC from different perspectives: HMPC has reduced constraint violations at the expense of increased electricity costs [12], has slightly inferior control performance but significantly reduced the computational expenses [13], and has improved the control objective at the expense of increased computational demand while preserving real-world applicability [14].

Explicit and implicit consideration of uncertainties can be combined by designing one of the layers of the HMPC as SMPC, resulting in hierarchical-stochastic MPC (HSMPC). However, the research on HSMPC is scarce in particular for building controls. Existing HSMPC studies have mostly concentrated on power systems such as the operation of a single grid-connected microgrid [15], the operation of multiple microgrids [16], and the economic dispatch of power systems under uncertainty [17]. For buildings, a three-layered HSMPC has been applied for the operation of heat pumps in power markets under price uncertainty [18], focusing on demand flexibility and electricity cost minimization.

Few papers have applied approaches similar to HSMPC to energy management in a single building with a photovoltaic (PV) system and a battery. Li and Wang [19] have proposed a two-time-scale stochastic control for optimal energy dispatch in a building equipped with PV, a battery, and electric chillers. The approach accounted for load and generation uncertainties and minimized electricity costs, while the effect on thermal comfort was not discussed. Mansy and Kwon [20] have applied a two-stage stochastic program for the optimal operation of an air conditioner under the integration of PV and a battery. The thermal building model has been designed as a single-zone model whose parameters are analytically determined and not identified based on an existing building. The stochastic optimization problem has been solved with a scenario generation approach considering uncertainty in price, solar irradiation, and ambient air temperature. The control performance was compared with an MPC using perfect forecasts and rule-based controls in terms of thermal comfort and electricity cost.

Overall, SMPC and HMPC have been applied to the control of heating systems in individual buildings with distributed energy resources. The results indicate that both controls result in improved thermal comfort. However, there has been little research on HSMPC. In addition, the existing studies on HSMPC and related approaches mostly focus on demand flexibility and electricity costs without considering thermal comfort. Furthermore, model inaccuracies are “almost never considered” [21] in the literature, although they can significantly influence the performance of model predictive controls [5,8].

1.1. Contributions

This paper proposes an HSMPC for the energy management of a single residential building with a PV system and a battery. The focus of the proposed control algorithm is to minimize the electricity cost while considering the thermal comfort of the occupants. For

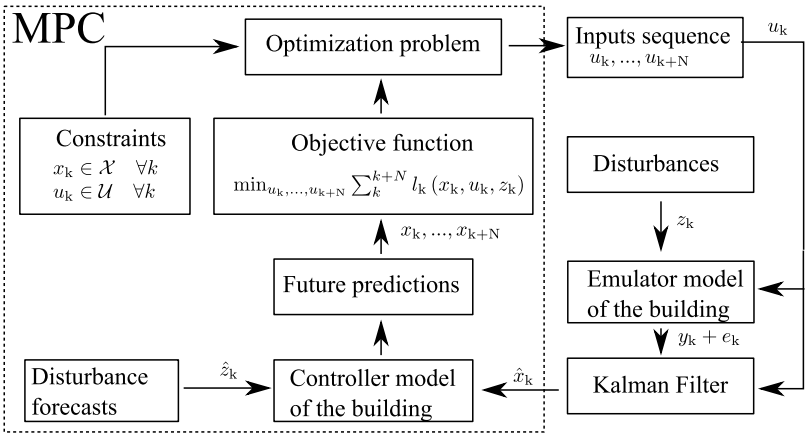

Fig. 1. Closed-loop system with MPC and state estimation.
Source: Adapted from [3].

the stochastic optimization, the statistical distributions of the uncertain variables are derived based on real forecast and measurement data.

Therefore, the major contributions of this paper include:

(i) HSMPC is designed for energy management in a residential building equipped with a heat pump for space conditioning and a PV-battery system.
(ii) The thermal building model is designed as a multi-zone model and identified from the operation data of a real building.
(iii) Model inaccuracies are considered in the control problem as additional noise on the controller model.
(iv) The performance of HSMPC is compared with DMPC, SMPC, and HMPC with respect to the electricity cost minimization and thermal comfort constraint violations.

1.2. Paper organization

The remainder of this paper is structured as follows: Section 2 introduces the individual models of the building's thermal behavior based on measurement data, the PV system, and the battery. In Section 3, the formulations and objective functions of DMPC, SMPC, HMPC, and HSMPC are introduced. Section 4 presents the identification of the thermal building models, the design of the Kalman filter, and the quantification of the errors of the solar radiation forecast, the ambient air temperature forecast, and the thermal building model inaccuracies. In Section 5, the case study for the controller comparison is introduced, and results are presented and discussed. The paper concludes in Section 6 with a review of the main results and an outlook for future work.

2. Component models

The closed-loop system for the present study is illustrated in Fig. 1. The current time step is denoted with k. The MPC uses disturbance forecasts $\hat{z}_k$ and a controller model of the building to predict the system's behavior over a finite number of time steps N and derives optimal inputs u to minimize an objective function l while simultaneously satisfying constraints $\mathcal{X}, \mathcal{U}$. The first of the derived inputs is applied to the emulator model, which emulates a real building and is therefore affected by additional disturbances z_k. In a real-world application, only noisy measurements are available. The outputs of the emulator model y_k are superposed with Gaussian measurement errors e_k to simulate the noisy measurements in real-world applications. Subsequently, a Kalman filter generates an estimate of the system's states $\hat{x}_k$ based on the controller model and the noisy measurements, which is used as the initial value for the next optimization step.

2.1. Building thermal models

Each room of the experimental building is modeled as an individual thermal zone to account for room-individual thermal preferences. A decentralized model structure is used (i.e. no thermal interactions between the rooms are considered). For a comparison between centralized and decentralized model structures, please refer to [22,23].

The inputs into the thermal models are the solar radiation $\dot{q}_s$ (W/m^2), ambient air temperature T_a (°C), and heat pump heat flow $\dot{Q}_{h,j}$ (W). The output of the thermal models is the room air temperature $T_{i,j}$ (°C). The index j indicates the room.

Two different thermal models are created: (i) a gray-box model used by the MPC as the controller model, and (ii) a black-box model used as the emulator model. The MPC utilizes the controller model to make predictions about the future thermal behavior of the building to derive optimal heating sequences of the heat pump. The emulator model is used to approximate the real building and its output is treated as the air temperature measurement. Using different models for the MPC and the emulator results in a model mismatch, which mimics the mismatch between the controller model and the true thermal behavior of the building.

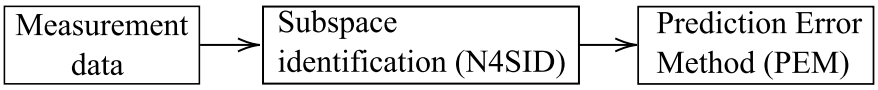

Fig. 2. Process to identify the black-box model.

2.1.1. Emulator model

Two methods are subsequently applied to identify the emulator model. First, a subspace identification method is used to provide an initial estimate of the thermal model's parameters. Then, a prediction error method is applied to refine the initial estimate (see Fig. 2). This procedure is recommended [24,25] because the prediction error method usually delivers superior identification results compared to the subspace method but it is more likely to get stuck in local minima [24].[1]

Two to three states per system output are recommended for a subspace identification method [26], although the subspace identification method could also estimate the appropriate model order itself. Accordingly, a model order of three is selected for each zone model since the only model output is the zone air temperature.[2]

2.1.2. Controller model

For the controller model, each thermal zone j is modeled with the following well-established model [6,27,28]:

$$C_{\mathrm{i,j}} \frac{\mathrm{d}T_{\mathrm{i,j}}}{\mathrm{d}t} = \frac{T_{\mathrm{m,j}} - T_{\mathrm{i,j}}}{R_{\mathrm{i,j}}} + \frac{T_{\mathrm{a}} - T_{\mathrm{i,j}}}{R_{\mathrm{a,j}}} + g_{\mathrm{s,j}} \dot{q}_{\mathrm{s}} + \dot{Q}_{\mathrm{h,j}} \tag{1}$$

$$C_{\mathrm{m,j}} \frac{\mathrm{d}T_{\mathrm{m,j}}}{\mathrm{d}t} = \frac{T_{\mathrm{a}} - T_{\mathrm{m,j}}}{R_{\mathrm{i,j}}} \tag{2}$$

where $T_{\mathrm{a}}, T_{\mathrm{i,j}}, T_{\mathrm{m,j}}$ represent the ambient air temperature, the indoor air temperature of zone j and the temperature of the thermal mass, respectively; $C_{\mathrm{i,j}}$ and $C_{\mathrm{m,j}}$ are the heat capacities of the indoor air and thermal mass; $R_{\mathrm{i,j}}$ and $R_{\mathrm{a,j}}$ are the thermal resistances between the indoor air and thermal mass and the ambient air and the indoor air, respectively; $\dot{q}_{\mathrm{s}}$ is the solar radiation and $g_{\mathrm{s,j}}$ is the solar heat gains factor.

State-space representation

The set of time-continuous differential equations as given by (1) and (2) can be discretized and restructured into an individual state-space representation for each thermal zone as follows

$$x_{\mathrm{k+1,j}} = A_{\mathrm{j}} x_{\mathrm{k,j}} + B_{\mathrm{j}} u_{\mathrm{k,j}} + E_{\mathrm{j}} z_{\mathrm{k}} \tag{3}$$

$$y_{\mathrm{k,j}} = C_{\mathrm{j}} x_{\mathrm{k,j}} \tag{4}$$

The state vector $x_{\mathrm{k,j}}$ contains the states of the jth room, $T_{\mathrm{i,j}}, T_{\mathrm{m,j}}$ at time k (see Eq. (5)). The input vector $u_{\mathrm{k,j}}$ represents the controllable input, which is the necessary electrical power consumption of the heat pump to emit the heat flow $\dot{Q}_{\mathrm{h,j}}$. The disturbance vector z_{k} contains the measurable disturbances, namely the ambient air temperature T_{a} and the global horizontal solar radiation $\dot{q}_{\mathrm{s}}$ which are identical for each room. The output vector $y_{\mathrm{k,j}}$ contains the room indoor air temperature $T_{\mathrm{i,j}}$ (see Eq. (6)):

$$x_{\mathrm{k,j}} = \begin{bmatrix} T_{\mathrm{i,k,j}} & T_{\mathrm{m,k,j}} \end{bmatrix} \tag{5}$$

$$y_{\mathrm{k,j}} = \begin{bmatrix} T_{\mathrm{i,k,j}} \end{bmatrix} \tag{6}$$

Temperature constraints are imposed to ensure the occupants' thermal comfort. The indoor air temperatures are softly constrained by:

$$T_{\mathrm{i,k,min,j}} - \xi_{\mathrm{k,j}} \leq T_{\mathrm{i,k,j}} \leq T_{\mathrm{i,k,max,j}} + \xi_{\mathrm{k,j}} \tag{7}$$

where $\xi_{\mathrm{k,j}}$ is a nonnegative slack variable to prevent numerical infeasibility.

2.2. Photovoltaic system

The photovoltaic power generation at time k is described according to [29]:

$$P_{\mathrm{PV,k}} = n_{\mathrm{module}} \cdot a_{\mathrm{module}} \cdot \eta_{\mathrm{STC}} \cdot \eta_{\mathrm{L\&T}} \cdot G_{\mathrm{k}} \cdot (1 - (\eta_{\mathrm{T}} \cdot (T_{\mathrm{a,k}} + \frac{NOCT - 20}{800} \cdot G_{\mathrm{k}} - T_{\mathrm{STC}}))) \tag{8}$$

with n_{module} as the number of photovoltaic modules, a_{module} as the area of a single module (m^2), η_{STC} as the efficiency of the module at standard testing conditions. $\eta_{\mathrm{L\&T}}$ denotes the combined efficiency of the inverter and the maximum power point tracking controller. G_{k} describes the incident solar irradiation falling on the PV module at time k ($\mathrm{W/m}^2$) and is calculated according to [30]. η_{T} refers to the temperature coefficient of efficiency (/K) and $T_{\mathrm{a,k}}$ to the ambient air temperature (°C) at time k. $NOCT$ represents the nominal operating cell temperature, and T_{STC} describes the temperature under standard normal conditions.

[1] The MATLAB commands *n4sid* and *pem* are applied to carry out the identification process.

[2] For more information on the algorithms, please refer to [25].

2.3. Battery storage system

The stored energy in the battery is modeled according to [6]:

$$E_{\mathrm{k}} = E_{\mathrm{k\text{-}1}} + \eta_{\mathrm{ch}} \cdot P_{\mathrm{ch,k}} \cdot t_{\mathrm{s}} - \frac{P_{\mathrm{d,k}}}{\eta_{\mathrm{d}}} \cdot t_{\mathrm{s}} \tag{9}$$

with E_{k} as the energy stored in the battery at the time step k, $P_{\mathrm{ch,k}}$ and $P_{\mathrm{d,k}}$ as charging and discharging power at the time step k, η_{ch} and η_{d} as charging and discharging efficiencies of the battery, and the sample time t_{s}. Furthermore, the state of charge of the battery is calculated according to:

$$SOC_{\mathrm{k}} = \frac{E_{\mathrm{k}}}{E_{\mathrm{max}}} \tag{10}$$

where E_{max} is the maximum energy that can be stored in the battery. The battery storage system is constrained by:

$$SOC_{\mathrm{min}} \leq SOC_{\mathrm{k}} \leq SOC_{\mathrm{max}} \tag{11}$$

$$0 \leq P_{\mathrm{ch,k}} \leq s_{\mathrm{ch,k}} \cdot P_{\mathrm{ch,max}} \tag{12}$$

$$0 \leq P_{\mathrm{d,k}} \leq s_{\mathrm{d,k}} \cdot P_{\mathrm{d,max}} \tag{13}$$

$$0 \leq s_{\mathrm{ch,k}} + s_{\mathrm{d,k}} \leq 1 \tag{14}$$

$$s_{\mathrm{ch,k}}, s_{\mathrm{d,k}} \in \{0, 1\} \tag{15}$$

where $s_{\mathrm{ch,k}}$ and $s_{\mathrm{d,k}}$ are binary variables indicating if charging or discharging occurs at the time step k. Eq. (14) prevents simultaneous charging and discharging of the battery.

2.4. Heat pump

The heating system of the building is a heat pump that consumes electrical energy to generate space heat. The efficiency of the heat pump's conversion of electrical energy to heat is given by its coefficient of performance ε:

$$\sum_{j} \dot{Q}_{\mathrm{h,j}} = \dot{Q}_{\mathrm{h}} = \varepsilon \cdot P_{\mathrm{HP}} \tag{16}$$

where P_{HP} is the electrical power consumption of the heat pump, $\dot{Q}_{\mathrm{h,j}}$ the heat flow emitted by the heat pump in each room j and $\dot{Q}_{\mathrm{h}}$ the total heat flow emitted by the heat pump.

The heat pump power satisfies the following:

$$0 \leq P_{\mathrm{HP,k,j}} \leq P_{\mathrm{HP,max,j}} \tag{17}$$

2.5. Energy system

All controllers have to satisfy energy conservation, i.e. the power consumption in the building must equal the sum of the power supplied by the grid, the battery, and the PV system. This is enforced by the following constraint:

$$P_{\mathrm{PV,k}} + P_{\mathrm{buy,k}} + P_{\mathrm{d,k}} = P_{\mathrm{ch,k}} + \sum_{j} P_{\mathrm{HP,k,j}} + P_{\mathrm{sell,k}} \tag{18}$$

where $\sum_j P_{\mathrm{HP,k,j}}$ is the power consumption of the heat pump, $P_{\mathrm{buy,k}}$ and $P_{\mathrm{sell,k}}$ are the bought and sold power from and to the grid. The power exchange with the grid is constrained by:

$$0 \leq P_{\mathrm{buy,k}} \leq s_{\mathrm{buy,k}} \cdot P_{\mathrm{buy,max}} \tag{19}$$

$$0 \leq P_{\mathrm{buy,k}} \leq s_{\mathrm{sell,k}} \cdot P_{\mathrm{sell,max}} \tag{20}$$

$$0 \leq s_{\mathrm{buy,k}} + s_{\mathrm{sell,k}} \leq 1 \tag{21}$$

$$s_{\mathrm{buy,k}}, s_{\mathrm{sell,k}} \in \{0, 1\} \tag{22}$$

where $P_{\mathrm{buy,max}}$ and $P_{\mathrm{sell,max}}$ are the respective maximum power that can be purchased or sold from and to the grid which is restricted by the power line capacity. $s_{\mathrm{buy,k}}$ and $s_{\mathrm{sell,k}}$ are binary variables (see Eq. (22)) indicating whether power is purchased from or sold to the grid at the time step k. For example, if $s_{\mathrm{buy,k}} = 0$ no power is purchased from the grid, and Eq. (19) collapses to $P_{\mathrm{buy,k}} = 0$. Conversely, if $s_{\mathrm{buy,k}} = 1$, power can be purchased from the grid and Eq. (19) becomes $0 \leq P_{\mathrm{buy,k}} \leq P_{\mathrm{buy,max}}$. Eq. (21) prevents simultaneous power purchasing and selling.

3. Model predictive control

The model predictive controller solves a constrained open-loop optimization problem based on the disturbance and price forecasts and the controller model outputs. This section describes the four different formulations of MPCs (i.e., deterministic, stochastic, hierarchical, hierarchical-stochastic) that are considered in the present paper. We define N as the number of time steps in the prediction horizon H, t_s as the sample time of the MPCs, and k as the current time step.

3.1. Deterministic model predictive control (DMPC)

DMPC does not explicitly consider uncertainties due to forecast errors and model inaccuracies. Therefore, DMPC may have significant constraint violations if the uncertainties are high. The advantages of DMPC lie in its simplicity in implementation because no information on the model and forecast accuracy needs to be collected.

The objective function is formulated as cost minimization (Eq. (23)), where the slack variables are penalized to prevent violations of the soft constraints.

$$\min \sum_{k}^{k+N} \left(\underbrace{t_s \cdot (P_{\text{buy,k}} \Omega_{\text{buy,k}} - P_{\text{sell,k}} \Omega_{\text{sell,k}})}_{\text{Cost of power transactions}} + \underbrace{\gamma \cdot \sum_{j} \|\xi_{\text{k,j}}\|_2}_{\text{Constraint violations}} \right) \tag{23}$$

subject to Eqs. (1)–(22)

where $\Omega_{\text{buy,k}}$ and $\Omega_{\text{sell,k}}$ are the prices for purchasing and selling power, $P_{\text{buy,k}}$ and $P_{\text{sell,k}}$ denote the purchased and sold power at time k. The parameter γ is a large number to penalize the constraint violations in each room j that are indicated by the slack variables $\xi_{\text{k,j}}$.

3.2. Stochastic model predictive control (SMPC)

Actual building temperatures differ from predicted temperatures for several reasons, including model inaccuracies and weather forecast errors. SMPC attempts to mitigate the effects of uncertainties by considering them explicitly in its controller model:

$$x_{\text{k+1,j}} = A_{\text{j}} x_{\text{k,j}} + B_{\text{j}} u_{\text{k,j}} + E_{\text{j}} z_{\text{k}} + F_{\text{j}} w_{\text{k,j}} \tag{24}$$

$$y_{\text{k,j}} = C_{\text{j}} x_{\text{k,j}} \tag{25}$$

where x, u, z, w, and y represent the states, controllable inputs, disturbance forecast, additive process noise representing model inaccuracies and weather forecast errors, and outputs (i.e. the indoor air temperatures $T_{\text{i,j}}$). The matrix F_{j} describes the influence of the additive noise w.

SMPC exploits knowledge about the statistical distribution of the noise w to avoid constraint violations with a certain probability. The temperature constraint (Eq. (7)) can be represented as the following probabilistic chance constraints:

$$\mathbb{P}(T_{\text{i,k,j}} = C_{\text{j}}(A_{\text{j}} x_{\text{k-1,j}} + B_{\text{j}} u_{\text{k-1,j}} + E_{\text{j}} z_{\text{k-1}} + F_{\text{j}} w_{\text{k-1,j}}) \geq T_{\text{i,k,min,j}}) = 1 - \alpha \tag{26}$$

$$\mathbb{P}(T_{\text{i,k,j}} = C_{\text{j}}(A_{\text{j}} x_{\text{k-1,j}} + B_{\text{j}} u_{\text{k-1,j}} + E_{\text{j}} z_{\text{k-1}} + F_{\text{j}} w_{\text{k-1,j}}) \leq T_{\text{i,k,max,j}}) = 1 - \alpha \tag{27}$$

The propagation of the uncertainties over the prediction horizon is expressed in the following matrix for each room j:

$$\mathbf{F}_{\text{j}} = \begin{bmatrix} F_{\text{j}} & 0 & \dots & 0 \\ A_{\text{j}} F_{\text{j}} & F_{\text{j}} & \dots & 0 \\ \vdots & \vdots & \ddots & \vdots \\ A_{\text{j}}^{N-1} F_{\text{j}} & A_{\text{j}}^{N-2} F_{\text{j}} & \dots & F_{\text{j}} \end{bmatrix} \tag{28}$$

Under the assumption of Gaussian noises, the chance constraints (26)–(27) can be reformulated to ensure a tractable optimization problem [31]:

$$T_{\text{i,k,j}} \geq T_{\text{i,k,min,j}} + \Phi^{-1}(1-\alpha) \sqrt{C_{\text{j}} F_{\text{k,j}} \mathbf{W}_{\text{k,j}} F_{\text{k,j}}^T C_{\text{j}}^T} - \xi_{\text{k,j}} \tag{29}$$

$$T_{\text{i,k,j}} \leq T_{\text{i,k,max,j}} - \Phi^{-1}(1-\alpha) \sqrt{C_{\text{j}} F_{\text{k,j}} \mathbf{W}_{\text{k,j}} F_{\text{k,j}}^T C_{\text{j}}^T} + \xi_{\text{k,j}} \tag{30}$$

where $\Phi^{-1}(\cdot)$ is the inverse cumulative probability function of the standard normal distribution, and $\mathbf{W}_{\text{k,j}}$ is the covariance matrix of the process noise of room j. The matrix $\mathbf{W}_{\text{k,j}}$ contains the variances of the uncertain variables and will also be used to design the Kalman filter in Section 4.2. $F_{\text{k,j}}$ represents the kth row of $\mathbf{F}_{\text{j}}$. The slack variables $\xi_{\text{k,j}}$ are added after the reformulation to avoid infeasibility, which is analogous to its use in Eq. (7).

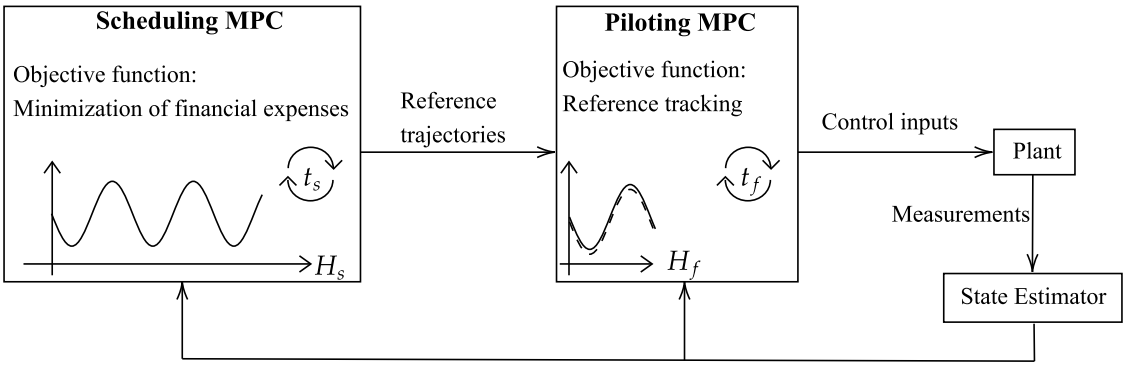

Fig. 3. Flowchart of a closed-loop hierarchical MPC.
Source: Adapted from [14].

The probability distribution of the uncertainties leads to probabilistic states. The expected values of the states are used to calculate the expected value of the objective function:

$$\min \mathbb{E}\left(\sum_{k}^{k+N}\left(\underbrace{t_s \cdot (P_{\text{buy,k}}\Omega_{\text{buy,k}} - P_{\text{sell,k}}\Omega_{\text{sell,k}})}_{\text{Cost of power transactions}} + \underbrace{\gamma \cdot \sum_{j=1}^{J} \|\xi_{\text{k,j}}\|_2}_{\text{Constraint violations}}\right)\right) \tag{31}$$

subject to Eqs. (1)–(6), (8)–(22), (29), (30)

3.3. Hierarchical model predictive control (HMPC)

Instead of explicitly accounting for uncertainties as in the SMPC, the impact of uncertainties can be mitigated implicitly by using a controller with a small sample time. A smaller sample time leads to a more frequent rescheduling of the MPC and thus to a faster response when constraints are violated.

However, an MPC with a long prediction horizon and a small sample time is computationally expensive. This computational burden can be alleviated by splitting the control problem into two layers, as presented in Fig. 3, leading to the HMPC approach.

The upper layer, the scheduling MPC, determines the cost-optimal schedules of the heat pump and battery over a long prediction horizon H_s (e.g., 24 h) and a comparatively large time step t_s (e.g., 15 min). The scheduling MPC can be designed as a DMPC or a SMPC and uses their respective objective functions (23) and (31). The lower layer, the piloting MPC (PMPC), implements the derived schedule, using a short prediction horizon H_f (e.g., 2 h) and a small sample time t_f (e.g., 5 min). The PMPC's short prediction horizon reduces its computational expenses and the small sample time ensures a quick response to constraint violations and deviations from the intended schedule. In contrast to the SMPC which explicitly considers uncertainties, the HMPC can only react after the constraints are violated and does not implement measures to avoid constraint violations preemptively.

The short prediction horizon of the PMPC would lead to poor results if the PMPC were to schedule the battery operation. This problem is addressed by forcing the PMPC to implement the schedules derived by the scheduling MPC. Thus, the following constraints are introduced:

$$P_{\text{ch,k,f}} = \hat{P}_{\text{ch,k,s}} \tag{32}$$

$$P_{\text{d,k,f}} = \hat{P}_{\text{d,k,s}} \tag{33}$$

$$P_{\text{sell,k,f}} = \hat{P}_{\text{sell,k,s}} \tag{34}$$

where $P_{\text{ch,k,f}}$, $P_{\text{d,k,f}}$, $P_{\text{sell,k,f}}$ are the decision variables (i.e. battery charging, battery discharging, power sold to the grid) of the PMPC that are set to the resampled schedule $\hat{P}_{\text{ch,k,s}}$, $\hat{P}_{\text{d,k,s}}$, $\hat{P}_{\text{sell,k,s}}$ as calculated by the scheduling MPC. The schedules have to be resampled because the scheduling MPC and the PMPC use different sample times. Eqs. (32) and (33) force the PMPC to implement the battery's schedule and Eq. (34) ensures that the PMPC sells the intended amount of power to the grid.

While the PMPC follows the schedules of the upper layer, it also requires a certain degree of freedom to be able to reschedule the heating system to react to temperature constraint violations. This is enabled with the following objective function:

$$\min \sum_{k}^{k+N_f}\left(\underbrace{\|P_{\text{buy,k,f}} - \hat{P}_{\text{buy,k,s}}\|_2 + \sum_{j}\|P_{\text{HP,k,f,j}} - \hat{P}_{\text{HP,k,s,j}}\|_2}_{\text{Cost of schedule deviations}} + \underbrace{\gamma \cdot \sum_{j}\|\xi_{\text{k,f,j}}\|_2}_{\text{Constraint violations}}\right) \tag{35}$$

Fig. 4. Considered building [23].

subject to Eqs. (1)–(22), (32)–(34)

The first two terms of the objective function constitute the cost of schedule deviations and are used to track the derived heat pump schedule. The third term penalizes constraint violations, causing the PMPC to deviate from the derived schedule if the temperature constraints are violated otherwise.

3.4. Hierarchical-stochastic model predictive control (HSMPC)

The proposed HSMPC combines the HMPC and SMPC by designing the scheduling MPC as SMPC. Consequently, for the scheduling MPC, the temperature constraints are recast as chance constraints (see Eqs. (29) and (30)) and the scheduling MPC uses the objective function of the SMPC (Eq. (31)). The PMPC considers the deterministic temperature constraints (Eq. (7)) and uses Eq. (35) as the objective function. Thus, the scheduling MPC plans to satisfy the temperature constraints with a certain probability while the piloting MPC can quickly react to constraint violations.

4. Identification of model parameters and uncertainties

The measurement data for the identification of the building thermal models are obtained from the "Living Lab" building at the KIT Energy Lab [32] (see Fig. 4). The considered facility is designed as a low-energy two-story residential building with a total living area of approximately 100 m^2, containing five rooms, a kitchen, and a bathroom. The building's envelope is constructed from aerated concrete with a thickness of 0.36 m, with a designed U-value of 0.23 $W/(m^2\,K)$. The roof, made of sandwich panels, has a designed U-value of 0.18 $W/(m^2\,K)$. The floor consists of 0.25 m of reinforced concrete and a Styrodur insulation layer of 0.1 m. The window-to-wall ratios for the north, east, south, and west facades are 20%, 3.5%, 13%, and 35%, respectively. The building is equipped with a rooftop photovoltaic system for energy generation and a battery for energy storage whose parameters are presented in Table 3. Space heating is generated by an air-source heat pump and distributed via radiators. To monitor indoor air temperatures, wall-mounted temperature sensors are installed in each room.

4.1. Identification of the thermal models

The emulator models are identified with two weeks of measurement data in winter, from Dec. 20, 2021, to Jan. 03, 2022. During this time, measurements are collected for the temperatures in each room, for the total heat emitted by the heating system, and for the global solar radiation, and the ambient air temperature. Since the total heat emitted by the heat pump $\dot{Q}_\mathrm{h}$ is measured but the room-individual heat flows $\dot{Q}_\mathrm{h,j}$ are required for the identification, $\dot{Q}_\mathrm{h,j}$ is approximated proportionally to the rooms air volume $V_\mathrm{i,j}$ [27]:

$$\dot{Q}_\mathrm{h,j} = \frac{V_\mathrm{i,j}}{\sum_j V_\mathrm{i,j}} \dot{Q}_\mathrm{h} \tag{36}$$

Table 1
RMSE of the five rooms for the controller models and emulator models in the validation period.

Room	RMSE	
	Emulator models	Controller models
1	0.43 K	0.35 K
2	0.15 K	0.25 K
3	0.19 K	0.37 K
4	0.30 K	0.33 K
5	0.33 K	0.36 K

Table 2
Values for the normal distributions of the measurement noises in each room.

Noise	Standard deviation in K	Mean in K
$w_{\text{meas},1}$	0.041	$1.71 \cdot 10^{-5}$
$w_{\text{meas},2}$	0.035	$4.2 \cdot 10^{-5}$
$w_{\text{meas},3}$	0.021	$1 \cdot 10^{-5}$
$w_{\text{meas},4}$	0.06	$2 \cdot 10^{-5}$
$w_{\text{meas},5}$	0.031	$3.1 \cdot 10^{-5}$

The controller models are trained on data generated by the emulator models since the emulator models emulate the real building in this study.

One week in January 2022 is used to validate the emulator and controller models. The emulator models are validated using temperature measurements of the building, while the controller models are validated using output data from the emulator models.

Table 1 presents the root mean square errors (RMSEs) for the validation period of the controller and emulator models. In each room, the RMSE is clearly below 1 K, indicating a sufficient model accuracy.

4.2. Design of the Kalman filter

The Kalman filter computes state estimates based on the controller models and noisy measurements. The process noise covariance matrix $Q_{\text{k,j}}$ at time k characterizes the uncertainties affecting the controller model of room j. The values of the matrices are time-varying because the solar radiation forecast is perfect at night but erroneous during the day. The ratio of $Q_{\text{k,j}}$ to the measurement noise covariance matrix R_{j} determines whether the Kalman filter relies more heavily on the controller model's output or the noisy measurements. The matrices R_{j} are time-independent since the measurement error is time-independent. The covariance matrices $Q_{\text{k,j}}$ and R_{j} are derived in the following sections to tune the Kalman filter.

4.2.1. Measurement noise covariance matrix R_j

In order to extract the measurement noise, undisturbed temperature measurements in each room are collected while the rooms are unoccupied. The measurement noise is smoothed out by filtering the raw temperature measurements with a moving average filter. Subsequently, the filtered measurements are subtracted from the raw measurements to extract the measurement noise. The statistical distribution of the measurement noise in each room is derived by fitting normal distributions.

Table 2 presents the standard deviations and mean values of the fitted normal distribution for the measurement noises of all five rooms. The mean values $\mu(w_{\text{meas,j}})$ are in the order of $\pm 10^{-5} \approx 0$ and are therefore approximated as zero.

4.2.2. Process noise covariance matrix $Q_{k,j}$

The process noise w (see Eq. (24)) includes weather forecast errors and the mismatch between the controller models and the emulator models. The covariance matrix of w is also required for the SMPC to reformulate its probabilistic constraints. The initial estimate for $Q_{\text{k,j}}$ is therefore selected as:

$$Q_{\text{k,j}} = \mathbf{W}_{\text{k,j}} \tag{37}$$

where $Q_{\text{k,j}}$ is the Kalman filter's process noise covariance matrix at time step k and $\mathbf{W}_{\text{k,j}}$ the process noise covariance matrix of the SMPC (see Eq. (30)). The initial estimate of $Q_{\text{k,j}}$ was further empirically fine-tuned to improve the performance of the Kalman filter.

4.3. Uncertainty quantification

In this section, the statistical distribution of the noises w is derived to obtain their covariance matrices $\mathbf{W}_{\text{k,j}}$. w includes three individual noises: (i) the ambient air temperature forecast error w_{amb}, (ii) the solar radiation forecast error w_{sol}, and (iii) the model error in each room $w_{\text{model,j}}$. In addition, for the reformulation of the chance constraints to be valid, the noises must satisfy two conditions:

- The noises w are normally distributed. Approximating a distribution as a normal one results in a non-significant error if the distribution's kurtosis and the absolute value of the skewness are below 7 and 2 respectively [33].

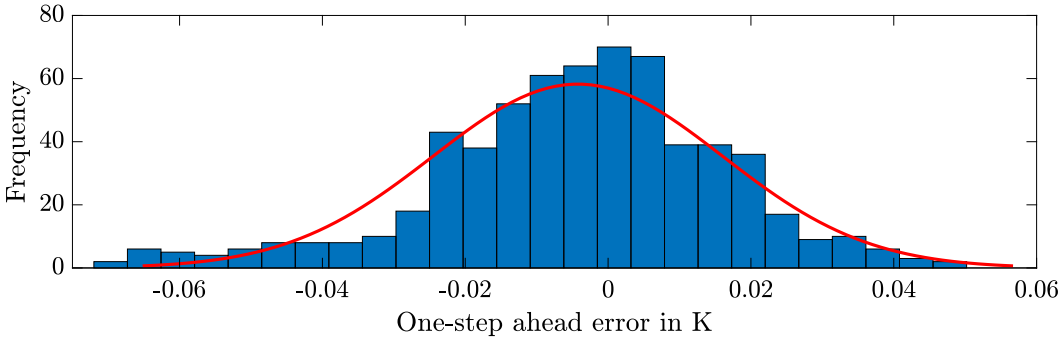

Fig. 5. One-step ahead error and fitted distribution for room 5.

- For each noise, the mean value of its normal distribution is zero.

These assumptions are verified in this section.

4.3.1. Weather forecast error

The statistical distributions of the forecast errors of the ambient air temperature and solar radiation are derived by comparing weather forecasts to measured data. The forecast data are retrieved from ECMWF [34] for Karlsruhe, Germany, and the measured data are obtained from the German Weather Service (DWD) [35] for the weather station in Rheinstetten. Both Karlsruhe and Rheinstetten are close to the location of the experimental building in Eggenstein-Leopoldshafen, with distances of about 8 and 15 kilometers, respectively. Based on the 12-hour forecast window, the forecast error is computed for six years (2015–2020).

The forecast error distributions for winter (December–February) are extracted and used, as the focus of this work is the heating period. Note that the forecast errors of solar radiation are calculated for each season and for night time and day time.

The forecast error distribution of the ambient air temperature has a mean value of $-0.066\,\mathrm{K}$, a standard deviation of $1.61\,\mathrm{K}$, a kurtosis of 4.47, and a skewness of -0.67. For the solar radiation forecast error distribution during the day, the mean value is $-23.15\,\mathrm{W/m^2}$, the standard deviation is $69\,\mathrm{W/m^2}$, the kurtosis is 4.4, and the skewness is -0.42. According to the values of the kurtosis and skewness for both distributions, assuming a normal distribution to model the forecast error is appropriate (kurtosis < 7, skewness < 2) [33]. Furthermore, the mean value of both extracted distributions is low ($-0.066\,\mathrm{K}$, $-23.15\,\mathrm{W/m^2}$) and therefore approximated with zero. During night time, no sun is shining and therefore the forecast error distribution of the solar radiation at night is modeled as a normal distribution with a mean value and standard deviation of zero.

4.3.2. Plant-model mismatch

The plant-model mismatch can be modeled as a noise acting on the state of the indoor air temperature [8]. The magnitude of the noise depends on the length of the simulation period [8] because errors accumulate over time. This means that a short-term prediction is more accurate than a long-term prediction. In this paper, the plant-model mismatch is captured by the one-step-ahead error, which is calculated as the difference between the outputs of the controller models and the emulator models for each MPC time step. At the end of each MPC time step, the indoor air temperature states of the controller models are reinitialized with those values calculated by the emulator model.

Without re-initialization, the error accumulates over the simulation period and does not equal the one-step-ahead error. The non-measurable state of the controller models, however, cannot be reinitialized. Thus, the first 40 entries of the one-step ahead error, corresponding to 10 h of simulation time, are discarded to allow the error in the initial condition of the non-measurable state to subside.

The one-step-ahead errors are tracked for a simulation over one week. Fig. 5 is an illustrative example that depicts the histogram of the one-step-ahead error and the fitted distribution for room 5.

The mean value of the derived distributions was small ($-0.004 < \mu(w_{\mathrm{model,j}}) < 0.0017$) and is therefore approximated as $\mu(w_{\mathrm{model,j}}) = 0$. Moreover, the values of the kurtosis and skewness indicate that the one-step ahead error in each room follows approximately a normal distribution according to [33]. Thus, the assumptions for the reformulation of the chance constraints are satisfied.

5. Evaluation of control strategies

5.1. Simulation settings

The results are obtained for the simulation period of one week (Dec. 28, 2015–Jan. 04, 2016). The weather forecasts are retrieved from ECMWF [34] and the weather measurements from DWD [35]. This week is selected because it contains days with high and low forecast errors, allowing for meaningful testing of the different controllers. The sample time of the DMPC, SMPC, and the scheduling

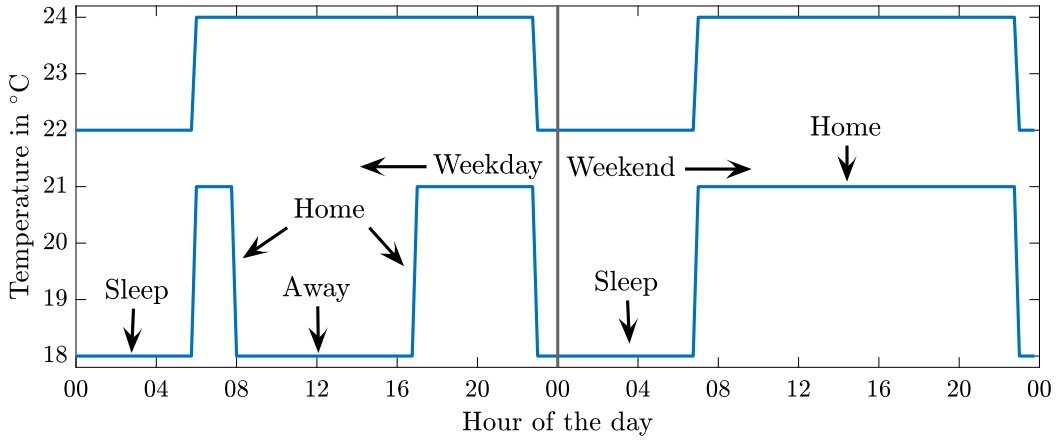

Fig. 6. Temperature constraints for the residential building case.

Table 3
Parameter values for the PV system and the battery.

Variable	Value	Variable	Value
η_T	0.005/K	SOC_{min}	10 %
$\eta_{I\&T}$	90 %	SOC_{max}	90 %
a_{module}	1.685 m^2	$P_{ch,max}$	3000 W
n_{module}	30	$P_{d,max}$	3000 W
$NOCT$	50 °C	η_d	93 %
T_{STC}	25 °C	η_{ch}	93 %
η_{STC}	19 %	E_{max}	19.5 kWh

layers of the HMPC and HSMPC is set to $t_s = 15$ min and their prediction horizon to $H_s = 24$ h. The sample time of the PMPC of the HMPC and HSMPC is set to $t_f = 5$ min and their prediction horizon to $H_f = 2$ h.

The considered building is constructed as a residential building and was built to study the interaction of the residential building sector with the power grid. Therefore, a temperature schedule for residential buildings is applied to reflect the intended use of the building. The occupancy schedule is based on data from over 20,000 smart thermostats and is retrieved from [36]. The schedule distinguishes occupant presence between 'home', 'away', and 'sleep' and between weekends and weekdays. However, the schedule provides temperature set points, whereas, in the context of MPC, a temperature range is preferred to increase demand flexibility. Therefore, lower and upper temperature constraints have to be determined. They are selected as follows to provide thermal comfort while simultaneously allowing demand flexibility:

$$T_{i,k,min,j} = \begin{cases} 21\,°C & \text{if home} \\ 18\,°C & \text{if away} \\ 18\,°C & \text{if sleep} \end{cases} \tag{38}$$

$$T_{i,k,max,j} = \begin{cases} 24\,°C & \text{if home} \\ 24\,°C & \text{if away} \\ 22\,°C & \text{if sleep} \end{cases} \tag{39}$$

The temperature schedules for weekdays and weekends are visualized in Fig. 6.

Since the considered building is equipped with a PV system and a battery, the numerical values are selected according to their technical specifications (see Table 3).

The price signal Ω_k^{buy} is retrieved from [37] and represents the wholesale electricity price in Germany from January 19, 2023, to January 26, 2023. Since this price does not reflect what a typical customer pays, it is rescaled so that the average price of the signal matches the actual retail price of electricity in Germany of 0.42 €/kWh. The price Ω_k^{sell} is assumed to be 0.086 €/kWh which is the current financial compensation for selling PV power to the grid in Germany [38]. Power can be sold to the grid by discharging the battery or by selling the power generated by the PV system.

The coefficient of performance ε is calculated based on the technical specifications of the manufacturer and depends on the ambient air temperature. The manufacturer provides a finite number of values of ε for different ambient air temperatures, which are linearly interpolated.

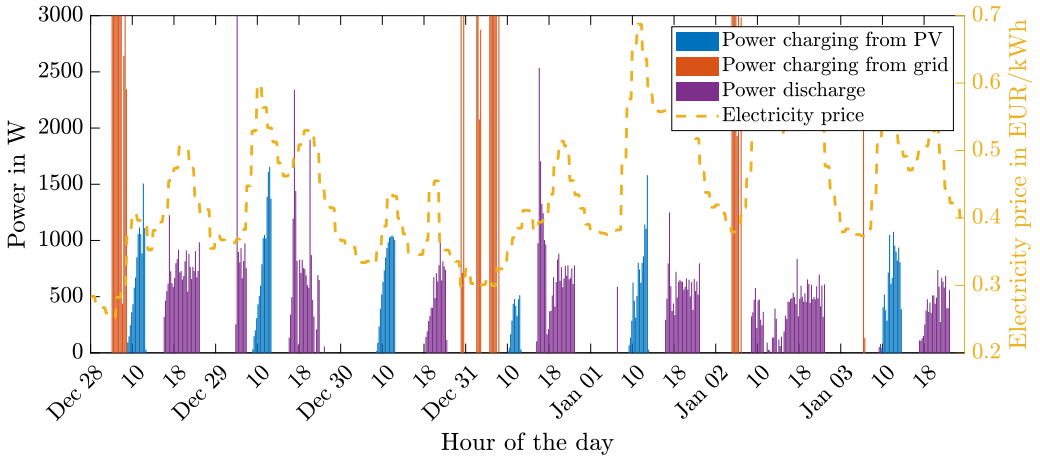

Fig. 7. The strategy of battery charging and discharging for cost minimization.

5.2. Key performance indicators

Three key performance indicators (KPIs) are used to evaluate the performance of different controllers. The KPIs represent the conflicting goals of thermal comfort and financial expenses that need to be reconciled. The first two KPIs evaluate the temperature constraint violations to assess occupant thermal comfort:

$$\Delta_{\mathrm{comfort,j}} = t_{\mathrm{s}} \sum_{k=1}^{M} d_{\mathrm{k,j}} \tag{40}$$

$$\bar{\Delta}_{\mathrm{comfort}} = \frac{1}{J} \sum_{j=1}^{J} \Delta_{\mathrm{comfort,j}} \tag{41}$$

$$d_{\mathrm{k,j}} = \begin{cases} T_{\mathrm{i,k,min,j}} - T_{\mathrm{i,k,j}} & \text{if} \quad T_{\mathrm{i,k,j}} < T_{\mathrm{i,k,min,j}} \\ T_{\mathrm{i,k,j}} - T_{\mathrm{i,k,max,j}} & \text{if} \quad T_{\mathrm{i,k,j}} > T_{\mathrm{i,k,max,j}} \\ 0 & \text{else} \end{cases} \tag{42}$$

The indicator $\Delta_{\mathrm{comfort,j}}$ reflects the thermal comfort violation at each individual room. It is calculated with the deviation from the upper or lower temperature constraint and the duration of the constraint violation (t_{s}). The indicator $\bar{\Delta}_{\mathrm{comfort}}$ evaluates the average comfort violation across all rooms.

The third KPI assesses the financial expenses:

$$\mathrm{cost} = t_{\mathrm{s}} \sum_{k=1}^{M} (P_{\mathrm{buy,k}} \Omega_{\mathrm{buy,k}} - P_{\mathrm{sell,k}} \Omega_{\mathrm{sell,k}}) \tag{43}$$

where M is the total number of time steps of the simulation period.

5.3. Deterministic MPC

DMPC is used as the benchmark and thus its results are presented first. In addition, we use DMPC to demonstrate the equipment scheduling capability of MPC because the cost-saving strategy of the DMPC is similar to that of other MPC formulations. The detailed comparison between different MPCs will be discussed later on in the following sections.

Fig. 7 presents the battery schedule as derived by the DMPC. The battery can be charged via two paths: (i) charging from the grid and (ii) charging from the PV. The MPC charges from the power grid when the electricity price is low. This can be observed on the first day at 06:00 in Fig. 7. Charging from the PV results in a recurring charging pattern that is visible every day around 10:00–15:00 as the MPC decides to store the generated power in the battery instead of selling it to the grid. The PV power can also be consumed immediately without being stored in the battery. However, because the temperature constraints are relaxed during the day when the occupants are assumed to be at work (see Fig. 6), heating is typically not required during these times, resulting in low power demand. Therefore, the PV produces more power than the power demand, and the excess power is stored in the battery.

In the early evening, the temperature constraints are tightened as occupants return home from work (see Fig. 6), leading to a high power demand due to the heat pump operation for space heating. Because the electricity price is usually high in the evening, the battery is discharged, subject to the SOC limits, to meet the heating demand and reduce the financial expenses. This can be observed, for example, from 17:00–23:00 on the first day.

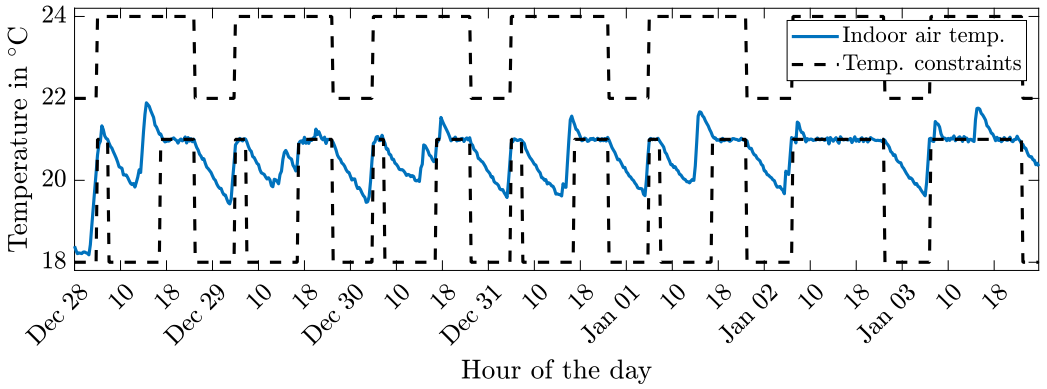

(a) Indoor air temperature in room 1.

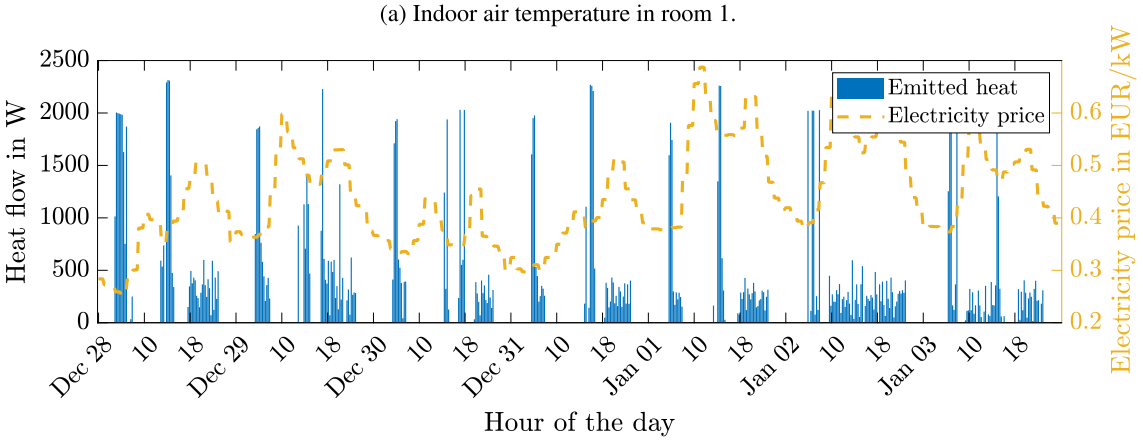

(b) Emitted heat by the heating system and corresponding electricity price in room 1.

Fig. 8. Heat pump operation for room 1.

Table 4
The thermal comfort violations in each room with the DMPC.

Room j	$\Delta_{\text{comfort,j}}$ in Kh
1	1.44
2	0.76
3	0.58
4	2.04
5	0.74
Average ($\bar{\Delta}_{\text{comfort}}$)	1.11

Besides the battery, the MPC can also schedule the heat pump. Fig. 8(a) presents the indoor air temperature calculated by the Kalman filter over the simulation period. The profiles of the heat supply to room 1 and the electricity price are shown in Fig. 8(b). Since the MPC behaves similarly in all rooms, it suffices to examine one room only.

Notably, at times when the electricity price is high, the DMPC aims to keep the indoor air temperature close to the lower temperature bound to reduce the heat pump power consumption and thus the financial expenses. When the electricity price is low (e.g., around 15:00 on the first day), the MPC strategically operates the heat pump to preheat the room as the MPC anticipates the higher temperature setpoint and electricity prices hours later (e.g., at 18:00). This preheating reduces the amount of heating required when the electricity price is high. After the preheat energy is used up, the MPC heats as little as possible to satisfy the temperature constraint if the electricity price is still high. This can be observed for example from 18:00–23:00 on the first day. During these times, the MPC eliminates the need for power purchase by discharging the battery (see Fig. 7).

Because the DMPC does not address weather forecast errors and model inaccuracies, comfort violations as indicated by Δ_{comfort} are observed in all five rooms (Table 4). Based on Ref. [4], the maximum acceptable comfort violations is 70 Kh/year. If the comfort violation is assumed to be evenly distributed over 52 weeks of a year, the comfort violation should satisfy $\Delta_{\text{comfort}} \leq 1.35$ Kh/week. Table 4 shows that rooms 1 and 4 do not meet the comfort requirement because their Δ_{comfort} values are higher than 1.35 Kh/week. However, the average comfort violation satisfies the comfort requirement.

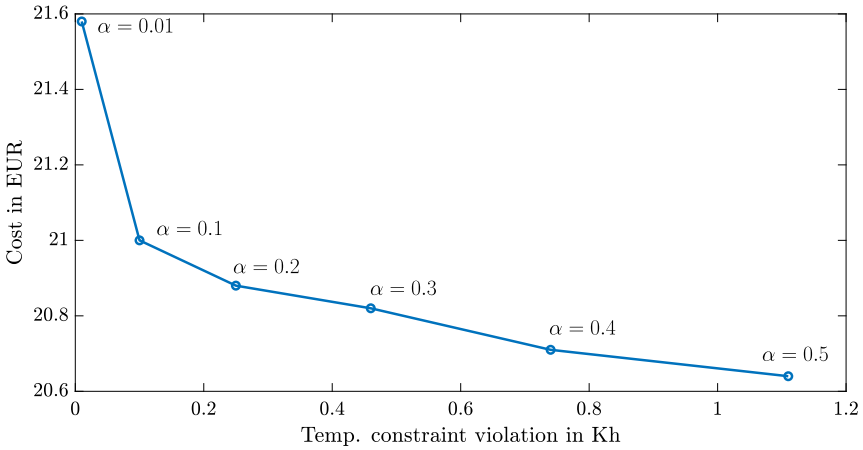

Fig. 9. Pareto front of the cost and average temperature constraint violations for the SMPC with multiple values of α.

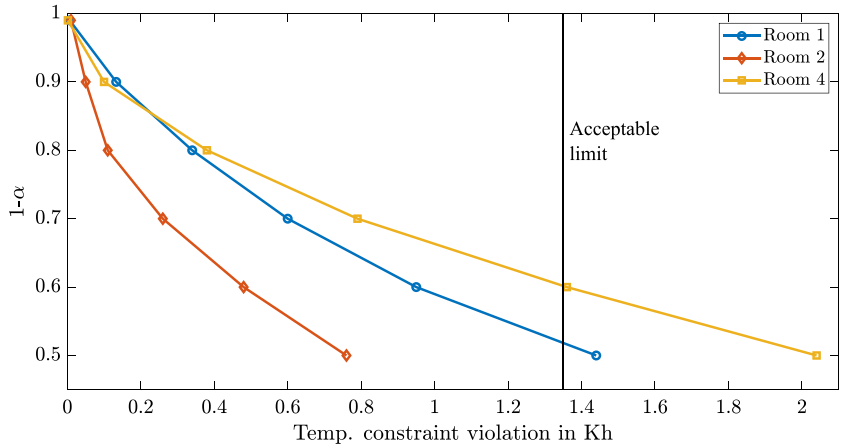

Fig. 10. Influence of α on the temperature constraint violations in rooms 1, 2, and 4.

5.4. Stochastic MPC

SMPC accounts for uncertainties by establishing a buffer zone to avoid potential violations of constraints. The size of the buffer zone is determined by the probability of constraint satisfaction $1-\alpha$. Decreasing the value of α leads to a larger buffer zone, resulting in higher power consumption and cost for heating. However, the larger buffer zone also reduces the temperature constraint violations. Fig. 9 shows the trade-off between cost and temperature constraint violations $\bar{\Delta}_{\text{comfort}}$ (averaged over all rooms) for varying α values.

In particular, at $\alpha = 0.5$, $\Phi^{-1}(0.5)$ is equal to zero (see Eq. (26)) and therefore, the SMPC performs equivalent to the DMPC. Fig. 9 clearly shows that the impact of α varies along the pareto front. For example, when the value of α is decreased from 0.5 (equivalent to DMPC) to 0.4, the comfort violation reduces from 1.1 Kh to 0.74 Kh (32.7%) while the cost increases by only €0.06 (0.3%). However, if the value of α is reduced from 0.1 to 0.01, the constraint violations reduce slightly from 0.11 Kh to 0.01 Kh (9% reduction of the total comfort violations of 1.11 Kh), while the cost increases by €0.6 (2.9%).

The average temperature constraint violations $\bar{\Delta}_{\text{comfort}}$ satisfy the acceptable threshold of $\Delta_{\text{comfort}} \leq 1.35$ Kh even in the DMPC. Considering that the threshold limit is violated under the DMPC for rooms 1 and 4 (see Table 4), it is worthwhile to investigate the thermal comfort conditions in individual rooms under SMPC. Therefore, the temperature constraint violations in rooms 1, 2, and 4 are plotted for multiple values of α in Fig. 10. Because rooms 3 and 5 behave similarly to room 2 and the discomfort in these rooms does not exceed the acceptable limit, those two rooms are not presented in Fig. 10.

Fig. 10 shows that the value of $1-\alpha = 0.6$ (i.e. $\alpha = 0.4$) suffices to reduce the comfort violation in room 1 to an acceptable level of 0.97 Kh but room 4 has its comfort violation of 1.37 Kh, which still slightly exceeds the acceptable limit of 1.35 Kh. If $\alpha \leq 0.3$, the constraint violation in all rooms is well below the acceptable limit.

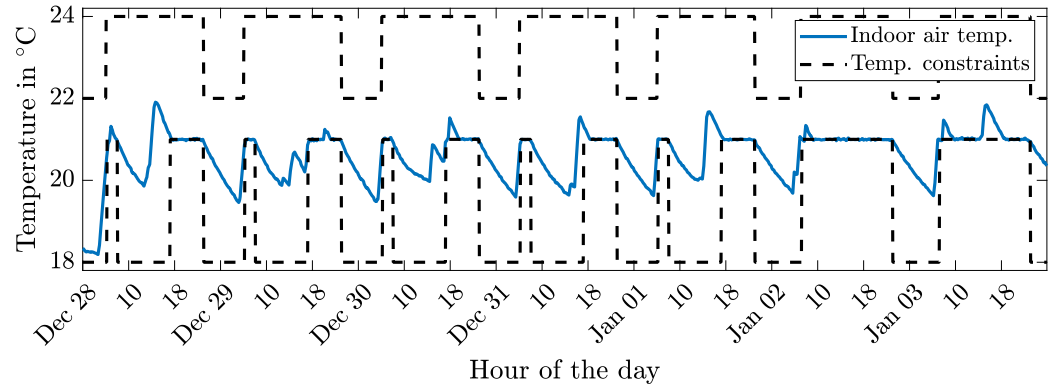

(a) Indoor air temperature in room 1 from the HMPC.

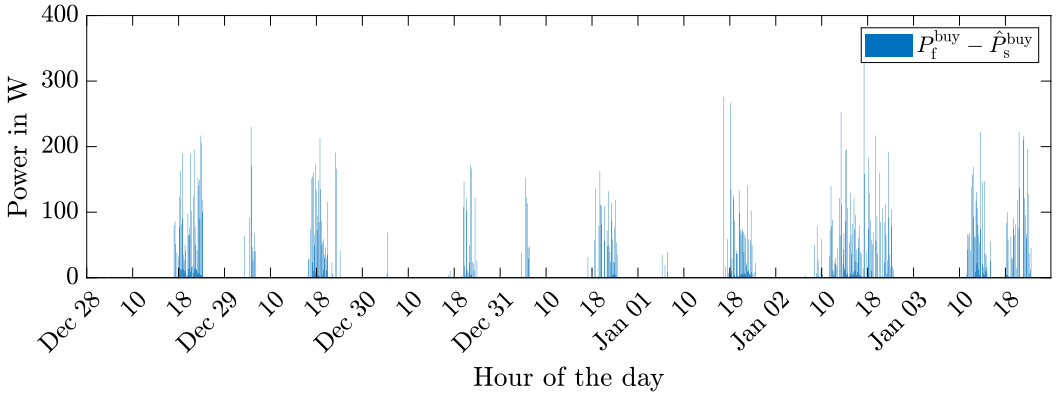

(b) Additional power bought by the PMPC.

Fig. 11. The working principle of the HMPC.

5.5. Hierarchical MPC

The HMPC consists of two levels of MPC: an upper layer with a long prediction horizon ($H_{\mathrm{s}} = 24\,\mathrm{h}$) and larger sample time ($t_{\mathrm{s}} = 15\,\mathrm{min}$) that calculates the cost-optimal schedule and a lower layer with a short prediction horizon ($H_{\mathrm{f}} = 2\,\mathrm{h}$) and small sample time ($t_{\mathrm{f}} = 5\,\mathrm{min}$). The small sample time of the lower level of the HMPC, the PMPC, can quickly react to the violation of constraints. If no constraint is violated, the PMPC follows the schedule derived from the upper layer of HMPC.

The working principle of HMPC is illustrated in Fig. 11, where the indoor air temperature in room 1 is depicted in Fig. 11(a) and the difference between the power that the PMPC purchased and the power that the scheduling MPC derived (i.e., $P_{\mathrm{buy,f}} - \hat{P}_{\mathrm{buy,s}}$) is presented in Fig. 11(b).

The PMPC follows the schedule exactly as long as the schedule derived by the scheduling MPC does not violate any constraints. This can be seen in Fig. 11, for example, on the first day until 18:00, when $P_{\mathrm{buy,f}} - \hat{P}_{\mathrm{buy,s}} = 0$ holds indicating that the PMPC follows the schedule exactly. Since the HMPC acts only after it detects the violation of constraints without taking preemptive measures, a recurring pattern can be observed in Fig. 11(b): the PMPC purchases additional power only when the scheduling MPC maintains the indoor air temperature close to the lower bound of comfort setting (between 18:00 and 23:00 for most days). The uncertainties cause the violation of thermal comfort constraints, which triggers the PMPC to purchase additional power to minimize its objective function.

Both the HMPC and the SMPC can reduce the violation of thermal comfort at the expense of cost increase. Their respective performance is compared in Fig. 12, including the comparison of cost in Fig. 12(a) and the comparison of energy consumption in Fig. 12(b).

The lower level of the HMPC uses one-third of the sample time of the DMPC and SMPC (5 min vs. 15 min) and can therefore react 67% quicker to constraint violations. The shorter response time results in a reduction of the temperature constraint violations of 67% from 1.1 Kh to 0.36 Kh in comparison to the DMPC. The cost increased by 1.7% from € 20.64 to € 20.99. For the same level of constraint violation as the HMPC, the SMPC needs to have $\alpha \approx 0.25$ and it achieves slightly less cost of approximately € 20.85.

On the other hand, the energy consumption from the HMPC is lower than that from the corresponding SMPC. This can be observed in Fig. 12(b) as the data point of the energy consumption of the HMPC is below the pareto front for the energy consumption of the SMPC.

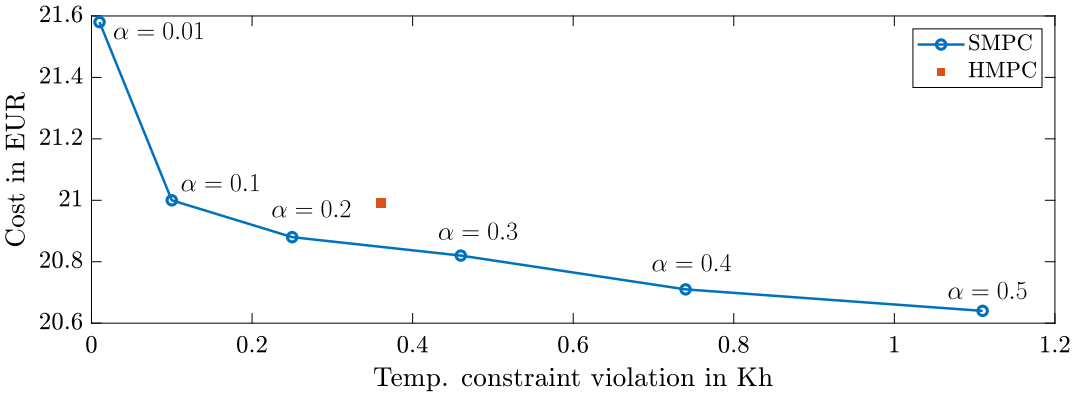

(a) Comparison of the resulting cost for the SMPC with multiple values for α and the HMPC.

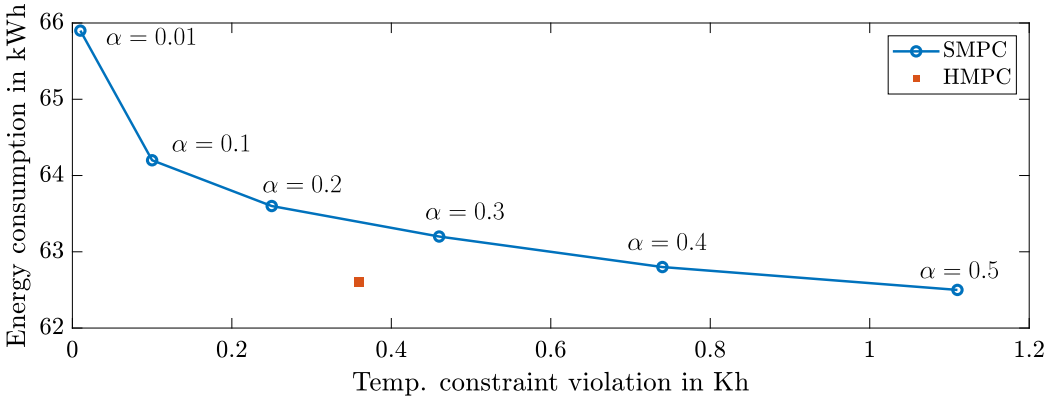

(b) Comparison of the resulting energy consumption for the SMPC with multiple values for α and the HMPC.

Fig. 12. Comparison of the SMPC and the HMPC.

5.6. Hierarchical-stochastic MPC

Both HMPC and SMPC can reduce the thermal comfort constraint violation from the DMPC at the expense of a slightly increased cost. The SMPC can achieve the same level of constraint violation at a lower cost than the HMPC, but with higher energy consumption, which can be explained by their different working principles. The HMPC reacts by purchasing power from the grid only after the constraint is violated. The power is purchased regardless of the electricity price because the violation of constraints is heavily penalized in the objective function. In other words, the HMPC consumes extra power compared to the DMPC if the constraint violation happens, but the extra power is not necessarily purchased when the electricity price is low. The SMPC, on the other hand, explicitly accounts for the uncertainties ahead by establishing a buffer zone to the temperature constraints. Establishing the buffer zone is considered in the optimization problem, and thus the SMPC can schedule space heating predominantly when the electricity price is low. However, once the comfort constraint is violated, the SMPC takes a longer time to react because its sample time is larger than the sample time of the HMPC.

Therefore, both HMPC and SMPC have their benefits and drawbacks. Their strengths can be combined by designing the upper level of the HMPC (i.e., the scheduling MPC) to be an SMPC, leading to the HSMPC formulation. This overcomes the issue that the HMPC cannot explicitly consider uncertainties and only reacts after the constraints violation happens. Meanwhile, the SMPC eliminates the need for a low value of α and the possible consequences of obtaining an excessively conservative solution because the PMPC detects constraint violations and takes necessary measures more frequently. Fig. 13 compares the results of the HMPC, SMPC, and HSMPC for multiple values of α.

For $\alpha = 0.4$, the HSMPC increases the costs negligibly by €0.05 (0.24%) relative to the SMPC while it reduces the comfort violation significantly by 0.53 Kh (72%). For $\alpha = 0.3$ and $\alpha = 0.2$, the HSMPC reduces the cost and thermal constraint violations simultaneously in comparison to the corresponding SMPC. Notably, the HSMPC has a more converged pareto front than the SMPC, which means that both the temperature constraint violation and the costs are less sensitive to the α value.

In comparison to the HMPC, the HSMPC with $\alpha = 0.4$, $\alpha = 0.3$, and $\alpha = 0.2$ respectively reduces the costs by €0.25 (1.2%), €0.21 (1%), and €0.18 (0.9%) and simultaneously reduces the temperature constraint violation by 0.16 Kh (44%), 0.29 Kh (81%), and 0.33 Kh (92%). The improved performance can be attributed to the explicit consideration of the uncertainties in the optimization,

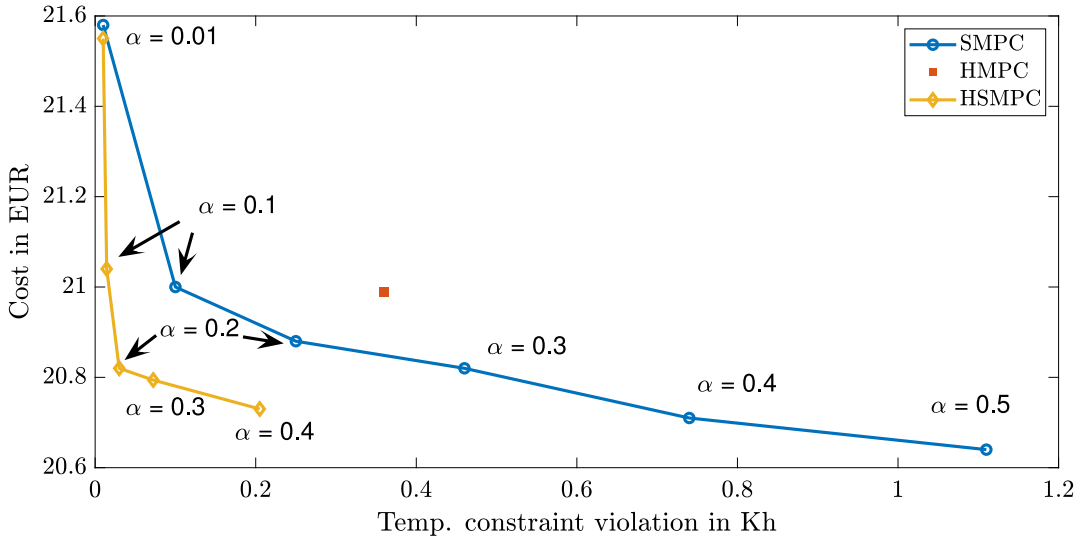

Fig. 13. Pareto front of the cost for the SMPC and HSMPC for multiple values for α and results of HMPC.

Table 5
Cost, average comfort violation, and room-individual comfort violation of DMPC, SMPC, HMPC, and HSMPC.

Control	α	Cost in €	$\bar{\Delta}_{\text{comfort}}$ in Kh	$\Delta_{\text{comfort},1}$ in Kh	$\Delta_{\text{comfort},2}$ in Kh	$\Delta_{\text{comfort},3}$ in Kh	$\Delta_{\text{comfort},4}$ in Kh	$\Delta_{\text{comfort},5}$ in Kh
DMPC	–	20.64	1.114	1.445	0.763	0.582	2.036	0.744
SMPC	0.01	21.58	0.010	0.006	0.007	0.013	0.002	0.024
	0.1	20.99	0.105	0.133	0.049	0.076	0.104	0.163
	0.2	20.88	0.252	0.343	0.114	0.161	0.376	0.269
	0.3	20.82	0.459	0.596	0.265	0.257	0.792	0.385
	0.4	20.71	0.743	0.948	0.480	0.395	1.364	0.528
HMPC	–	20.99	0.355	0.519	0.223	0.105	0.709	0.221
HSMPC	0.01	21.55	0.010	0.006	0.007	0.013	0.002	0.024
	0.1	21.04	0.014	0.045	0	0	0.003	0.023
	0.2	20.82	0.031	0.080	0.006	0.006	0.019	0.045
	0.3	20.79	0.072	0.141	0.016	0.026	0.085	0.093
	0.4	20.73	0.205	0.314	0.096	0.073	0.391	0.151

leading to improved heat pump scheduling. For a complete overview of the control results of all four controllers (i.e. DMPC, SMPC, HMPC, HSMPC) see Table 5.

6. Conclusion

The present work proposes a novel hierarchical-stochastic model predictive control (HSMPC) to mitigate the impact of uncertain weather forecasts and model inaccuracies on cost minimization and thermal comfort. While model inaccuracies are often neglected in the literature, in this work they are considered as additional noise on the controller model. The performance of the proposed control method is compared with three conventional MPC approaches (i) deterministic MPC (DMPC), (ii) stochastic MPC (SMPC), and (iii) hierarchical MPC (HMPC) in a one-week winter simulation study for a residential building in Germany. The control problem includes a heat pump, a battery, and a photovoltaic system, and the thermal behavior of the building is captured with a multi-zone thermal building model. Major findings of this work are summarized below.

- With the DMPC, the averaged comfort (across all rooms) is not jeopardized. However, the discomfort threshold is exceeded in two rooms, highlighting the importance of multi-zone modeling.
- For the SMPC, the trade-off between comfort violations and cost can be selected by tuning the probability of constraint satisfaction $1-\alpha$. A high value of α is beneficial for cost minimization but may cause unacceptable thermal comfort problems. Similarly, a low value of α is beneficial for thermal comfort but has a high cost.
- The HMPC has slightly increased the cost in comparison to the SMPC with a similar level of comfort violations. The HMPC consumes less energy but a higher energy cost is incurred because of the power consumption at high-price times.
- The HSMPC combines the explicit consideration of the uncertainties from the SMPC with the small sample time from the HMPC, leading to lower costs and lower temperature constraint violation than the HMPC and SMPC applied separately.

Overall, SMPC and HMPC are successfully combined to formulate the HSMPC. HSMPC performs superior to SMPC and HMPC individually with respect to the minimization of electricity cost and temperature constraint violation. The results are expected to be generalizable to other building configurations since the distribution of RC parameters of thermal building models is not influenced by building characteristics [39]. Similarly, the influence of varying climates on the building model is small [39], suggesting that the results are valid across climates.

While HSMPC combines the advantages of SMPC and HMPC, it also combines their disadvantages. Both the considerable modeling effort of SMPC due to uncertainty quantification and the higher computational effort of HMPC due to cascading of two controllers affect HSMPC. Furthermore, the presented approach relies on the reformulation of chance constraints, which are tractable only if the uncertain variables follow certain distributions. Consequently, future work can investigate HSMPC with scenario sampling approaches that do not require assumptions about the distributions of the uncertain variables. For a more accurate quantification of thermal comfort, dedicated indicators such as the Predicted Mean Vote can be considered. Other directions for future work include the energy management of a building cluster, the integration of hot water tank charging and electric vehicle charging into the control concept.

CRediT authorship contribution statement

Felix Langner: Conceptualization, Software, Writing – review & editing, Writing – original draft, Visualization, Validation, Methodology, Investigation. **Moritz Frahm:** Supervision, Writing – review & editing, Writing – original draft, Methodology, Investigation, Conceptualization. **Weimin Wang:** Conceptualization, Methodology, Writing – review & editing, Writing – original draft, Supervision. **Jörg Matthes:** Conceptualization, Writing – review & editing, Supervision, Resources, Methodology. **Veit Hagenmeyer:** Conceptualization, Funding acquisition, Writing – review & editing, Supervision, Resources.

Declaration of competing interest

The authors declare that they have no known competing financial interests or personal relationships that could have appeared to influence the work reported in this paper.

Data availability

Data will be made available on request.

Acknowledgments

We acknowledge the financial support of the Helmholtz Association of German Research Centres (HGF) within the framework of the Program-Oriented Funding POF IV in the program Energy Systems Design (ESD, project number 37.12.01).

References

[1] IEA, Transition to sustainable buildings, 2013, https://www.iea.org/reports/transition-to-sustainable-buildings. (Accessed 10 June 2023).
[2] P. Kohlhepp, H. Harb, H. Wolisz, S. Waczowicz, D. Müller, V. Hagenmeyer, Large-scale grid integration of residential thermal energy storages as demand-side flexibility resource: A review of international field studies, Renew. Sustain. Energy Rev. 101 (2019) 527–547, http://dx.doi.org/10.1016/j.rser.2018.09.045.
[3] J. Drgoňa, J. Arroyo, I. Cupeiro Figueroa, D. Blum, K. Arendt, D. Kim, E.P. Ollé, J. Oravec, M. Wetter, D.L. Vrabie, L. Helsen, All you need to know about model predictive control for buildings, Annu. Rev. Control 50 (2020) 190–232, http://dx.doi.org/10.1016/j.arcontrol.2020.09.001.
[4] F. Oldewurtel, A. Parisio, C.N. Jones, D. Gyalistras, M. Gwerder, V. Stauch, B. Lehmann, M. Morari, Use of model predictive control and weather forecasts for energy efficient building climate control, Energy Build. 45 (2012) 15–27, http://dx.doi.org/10.1016/j.enbuild.2011.09.022.
[5] A. Uytterhoeven, R. Van Rompaey, K. Bruninx, L. Helsen, Chance constrained stochastic mpc for building climate control under combined parametric and additive uncertainty, J. Build. Perform. Simul. 15 (3) (2022) 410–430.
[6] H. Nagpal, I.-I. Avramidis, F. Capitanescu, P. Heiselberg, Optimal energy management in smart sustainable buildings – a chance-constrained model predictive control approach, Energy Build. 248 (2021) 111163, http://dx.doi.org/10.1016/j.enbuild.2021.111163.
[7] X. Wang, Y. Liu, L. Xu, J. Liu, H. Sun, A chance-constrained stochastic model predictive control for building integrated with renewable resources, Electr. Power Syst. Res. 184 (2020) 106348, http://dx.doi.org/10.1016/j.epsr.2020.106348.
[8] A. Amadeh, Z.E. Lee, K.M. Zhang, Quantifying demand flexibility of building energy systems under uncertainty, Energy 246 (2022) 123291.
[9] F. Langner, W. Wang, M. Frahm, V. Hagenmeyer, Model predictive control of distributed energy resources in residential buildings considering forecast uncertainties, Energy Build. 303 (2024) http://dx.doi.org/10.1016/j.enbuild.2023.113753.
[10] Y. Yao, D.K. Shekhar, State of the art review on model predictive control (mpc) in heating ventilation and air-conditioning (hvac) field, Build. Environ. 200 (2021) 107952, http://dx.doi.org/10.1016/j.buildenv.2021.107952.
[11] C.R. Touretzky, M. Baldea, Integrating scheduling and control for economic MPC of buildings with energy storage, J. Process Control 24 (8) (2014) 1292–1300, http://dx.doi.org/10.1016/j.jprocont.2014.04.015.
[12] A. Lefort, R. Bourdais, G. Ansanay-Alex, H. Guéguen, Hierarchical control method applied to energy management of a residential house, Energy Build. 64 (2013) 53–61, http://dx.doi.org/10.1016/j.enbuild.2013.04.010.
[13] A. Abreu, R. Bourdais, H. Guéguen, Hierarchical model predictive control for building energy management of hybrid systems, IFAC-PapersOnLine 51 (16) (2018) 235–240, http://dx.doi.org/10.1016/j.ifacol.2018.08.040.
[14] M. Mork, A. Xhonneux, D. Müller, Hierarchical model predictive control for complex building energy systems, Bauphysik 42 (6) (2020) 306–314, http://dx.doi.org/10.1002/bapi.202000031.
[15] S. Raimondi Cominesi, M. Farina, L. Giulioni, B. Picasso, R. Scattolini, A two-layer stochastic model predictive control scheme for microgrids, IEEE Trans. Control Syst. Technol. 26 (1) (2018) 1–13, http://dx.doi.org/10.1109/TCST.2017.2657606.

[16] P. Kou, D. Liang, L. Gao, Distributed EMPC of multiple microgrids for coordinated stochastic energy management, Appl. Energy 185 (2017) 939–952, http://dx.doi.org/10.1016/j.apenergy.2016.09.092.
[17] M.A. Velasquez, N. Quijano, A.I. Cadena, M. Shahidehpour, Distributed stochastic economic dispatch via model predictive control and data-driven scenario generation, Int. J. Electr. Power Energy Syst. 129 (2021) 106796, http://dx.doi.org/10.1016/j.ijepes.2021.106796.
[18] H. Golmohamadi, K.G. Larsen, P.G. Jensen, I.R. Hasrat, Hierarchical flexibility potentials of residential buildings with responsive heat pumps: A case study of Denmark, J. Build. Eng. 41 (2021) 102425, http://dx.doi.org/10.1016/j.jobe.2021.102425.
[19] H. Li, S. Wang, Two-time-scale coordinated optimal control of building energy systems for demand response considering forecast uncertainties, Energy 253 (2022) http://dx.doi.org/10.1016/j.energy.2022.124204.
[20] H. Mansy, S. Kwon, Optimal HVAC control for demand response via chance-constrained two-stage stochastic program, IEEE Trans. Smart Grid 12 (3) (2021) 2188–2200, http://dx.doi.org/10.1109/TSG.2020.3037668, conference Name: IEEE Transactions on Smart Grid.
[21] H. Thieblemont, F. Haghighat, R. Ooka, A. Moreau, Predictive control strategies based on weather forecast in buildings with energy storage system: A review of the state-of-the art, Energy Build. 153 (2017) 485–500, http://dx.doi.org/10.1016/j.enbuild.2017.08.010.
[22] J. Arroyo, F. Spiessens, L. Helsen, Identification of multi-zone grey-box building models for use in model predictive control, IBPSA J. Build. Perform. Simul. 13 (4) (2020) 472–486, http://dx.doi.org/10.1080/19401493.2020.1770861.
[23] M. Frahm, E. Klumpp, S. Meisenbacher, J. Matthes, R. Mikut, V. Hagenmeyer, Development and validation of grey-box multi-zone thermal building models, in: BauSIM2022-9. Deutsch-ÖSterreichische IBPSA-Konferenz: Tagungsband, International Building Performance Simulation Association, 2022, http://dx.doi.org/10.26868/29761662.2022.22.
[24] M.D. Knudsen, L. Georges, K.S. Skeie, S. Petersen, Experimental test of a black-box economic model predictive control for residential space heating, Appl. Energy 298 (2021) 117227, http://dx.doi.org/10.1016/j.apenergy.2021.117227.
[25] L. Ljung, System identification, in: Signal Analysis and Prediction, Springer, 1998, pp. 163–173.
[26] S. Prívara, J. Cigler, Z. Váňa, F. Oldewurtel, C. Sagerschnig, E. Žáčeková, Building modeling as a crucial part for building predictive control, Energy Build. 56 (2013) 8–22, http://dx.doi.org/10.1016/j.enbuild.2012.10.024.
[27] M. Frahm, S. Meisenbacher, E. Klumpp, R. Mikut, J. Matthes, V. Hagenmeyer, Multi-zone grey-box thermal building identification with real occupants, in: Proceedings of the 9th ACM International Conference on Systems for Energy-Efficient Buildings, Cities, and Transportation, BuildSys '22, Association for Computing Machinery, New York, NY, USA, 2022, pp. 484–487, http://dx.doi.org/10.1145/3563357.3567403.
[28] H. Madsen, J. Holst, Estimation of continuous-time models for the heat dynamics of a building, Energy Build. 22 (1) (1995) 67–79, http://dx.doi.org/10.1016/0378-7788(94)00904-X.
[29] M.J.M. Al Essa, Home energy management of thermostatically controlled loads and photovoltaic-battery systems, Energy 176 (2019) 742–752, http://dx.doi.org/10.1016/j.energy.2019.04.041.
[30] Jadwa Beckman, Solar Engineering of Thermal Processes, third ed., John Wiley & sons, Hoboken, New Jersey, 2006.
[31] M. Farina, L. Giulioni, R. Scattolini, Stochastic linear model predictive control with chance constraints – A review, J. Process Control 44 (2016) 53–67, http://dx.doi.org/10.1016/j.jprocont.2016.03.005.
[32] V. Hagenmeyer, H. Kemal Çakmak, C. Düpmeier, T. Faulwasser, J. Isele, H.B. Keller, P. Kohlhepp, U. Kühnapfel, U. Stucky, S. Waczowicz, R. Mikut, Information and communication technology in energy lab 2.0: Smart energies system simulation and control center with an open-street-map-based power flow simulation example 4 (1), 2016, pp. 145–162, http://dx.doi.org/10.1002/ente.201500304.
[33] H.-Y. Kim, Statistical notes for clinical researchers: Assessing normal distribution (2) using skewness and kurtosis, Restor. Dent. Endod. 38 (1) (2013) 52–54, http://dx.doi.org/10.5395/rde.2013.38.1.52.
[34] ECMWF, 2022, https://www.ecmwf.int/en/forecasts. (Accessed 26 August 2022).
[35] German weather service, 2022, https://www.dwd.de/EN/Home/home_node.html. (Accessed 26 August 2022).
[36] T. Ueno, A. Meier, A method to generate heating and cooling schedules based on data from connected thermostats, Energy Build. 228 (2020) 110423, http://dx.doi.org/10.1016/j.enbuild.2020.110423.
[37] Bundesnetzagentur, Smard strommarktdaten, 2023, URL https://www.smard.de/home/downloadcenter/download-marktdaten. (Last Accessed 29 January 2023).
[38] Bundesnetzagentur, EEG-Registerdaten und -Fördersätze, 2023, URL https://www.bundesnetzagentur.de/DE/Fachthemen/ElektrizitaetundGas/ErneuerbareEnergien/ZahlenDatenInformationen/EEG_Registerdaten/start.html. (Last accessed 20 January 2023).
[39] C. Vallianos, J. Candanedo, A. Athienitis, Thermal modeling for control applications of 60 000homes in North America using smart thermostat data, Energy Build. 303 (2024) 113811, http://dx.doi.org/10.1016/j.enbuild.2023.113811.